Experimental Verification of Optimal Flux Weakening in Surface PM Machines Using Concentrated Windings

Ayman M. EL-Refaie
elrefaie@cae.wisc.edu

Thomas M. Jahns
jahns@engr.wisc.edu

Patrick J. McCleer
pat@mccleerpower.com

John W. McKeever
mckeeverjw@ornl.gov

Department of Electrical and Computer Engineering
University of Wisconsin – Madison
Madison, WI USA

McCleer Power, Inc.
Jackson, MI USA

Oak Ridge National Laboratory
Oak Ridge, TN USA

Abstract — **Previous analytical work has shown that it is possible to design surface PM (SPM) machines using fractional-slot concentrated windings to achieve wide speed ranges of constant power operation by satisfying the optimal flux-weakening condition. This paper presents a 6kW 36-slot/30-pole concentrated winding prototype SPM machine that has been designed using a closed-form analytical technique developed specifically for this class of machines. Experimental testing of this machine has been carried out to determine its performance capabilities, including flux-weakening operation. Detailed comparisons between analytical, finite element analysis (FEA), and experimental results are presented that confirm the ability of fractional-slot concentrated winding SPM machines to achieve their high-speed operating objectives. Important issues including the machine's back-emf voltage at top speed, eddy current losses in the magnets, and inverter performance are analyzed and discussed in detail.**

Keywords- flux weakening; synchronous; permanent magnet; surface; concentrated; fractional-slot; windings; experimental; verification.

I. INTRODUCTION

Past investigations have shown that wide speed ranges of constant-power operation can be achieved using surface PM (SPM) machines by introducing fractional-slot concentrated windings to reduce the machine's characteristic current [1]. A closed-form analytical technique has been developed that provides an effective means for rapidly analyzing candidate SPM machine designs using concentrated windings and tuning them to achieve the critical condition for optimal flux weakening [2].

The ability of designers to use fractional-slot concentrated windings to reduce the SPM machine's characteristic current sufficiently to significantly expand the machine's high-speed operating capabilities has appeared only recently in the technical literature [3]. There are very few examples of experimental machines exhibiting these characteristics that
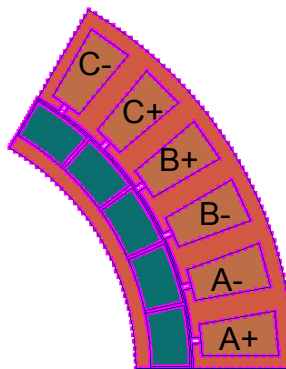
Figure 1: Basic repeating unit of prototype SPM machine consisting of 6 stator slots and 5 poles

have been tested and then documented in technical forums for the broad professional community [4].

This paper presents a 6kW 36-slot/30-pole concentrated winding prototype machine that has been designed using this analytical technique. Experimental testing of this machine has been carried out to evaluate its performance capabilities, including flux-weakening operation. Detailed comparisons between analytical, finite element analysis (FEA), and experimental results are presented in this paper. A wide range of the machine's parameters and operating characteristics are presented to help interested readers to assess the strengths and limitations of this class of machine. This discussion will include lessons learned by the authors – some unexpected – during the course of this development effort.

II. ANALYTICAL AND FINITE ELEMENT ANALYSIS RESULTS

A. Machine Dimensions and Parameters

A fractional-slot concentrated winding SPM machine has been designed for a wide speed range of constant-power operation using the analytical technique presented in [2]. A section of the 36-slot/30-pole machine (slot/pole/phase = 2/5) is shown in Fig. 1 [1]. The objective of this development effort has been to design the SPM machine to achieve a high constant power speed ratio (CPSR) with a target value of 10:1. Using the requirements for an automotive starter/alternator application as a reference point [5], the machine was originally

designed as a motor to deliver 4kW at a base speed of 600 r/min and 6 kW at the top speed of 6000 r/min. All of the analytical results have been verified using finite element analysis (MagNet2D by Infolytica Corp.).

The basic machine unit consisting of 6 stator slots and 5 rotor poles is shown in Figure 1. Key parameters and dimensions for the machine stator and rotor are presented in Table I and Table II, respectively. Calculated inductance values for the machine are provided in Table III. Important machine parameters related to the machine's field weakening capabilities, including the rated and characteristic current values, are presented in Table IV. Table V provides information about the machine's mass, including a breakdown by material.

There are several important observations that can be made from the entries in these tables. Bonded neodymium-iron-boron magnets were selected for this prototype machine. The design value of the magnet remanent flux density B_r is 0.55 T with a relative permeability μ_r of 1.22, using the magnet characteristics at 100°C in order to include temperature effects and to avoid demagnetization. The reason for choosing bonded magnets with a lower B_r value is to minimize the eddy-current losses in the magnets that will be discussed in more detail in Section III. The adoption of such relatively low-strength magnets explains the choice of a relatively large magnet depth of 13mm.

B. Machine Inductances and Flux Weakening Operation

The self- and mutual inductance components in Table III (including harmonic leakage inductance) have been calculated using the winding function approach [6]. The slot leakage component is the dominant inductance component, attributable to the adoption of such a large effective air gap length (14mm).

It can be seen in Table IV that this machine has a calculated flux-weakening index *FWI* value (defined as the ratio of the machine's characteristic current I_{ch} to its rated current I_R) that is less than unity (0.79) even though the design was initially tuned to achieve unity. This indicates that the machine deviates somewhat from the optimal flux-weakening condition, reflecting an oversight that occurred during the design process. More specifically, the slot leakage inductance was initially calculated using classical formulae that are appropriate for ac machines such as induction machines [7]. Unfortunately, such formulae become progressively inaccurate as the machine effective air gap increases, resulting in a calculated total phase self-inductance that is approx. 25% larger than the target value. It is noted, with some irony, that the design effort to increase the machine's inductance (in order to reduce the characteristic current) was *too* successful in this case.

Since discovering this error, more accurate 2-D models have been incorporated into the analytical model for calculating the slot leakage inductance in surface SPM machines with large effective air gaps [8-10]. Entries in both Tables III and IV are calculated using this improved model. This same model has been used to explore the changes that would be necessary in

TABLE I: Stator Dimensions and Winding Data for the 36-slot/30-pole SPM Machine

Number of slots	36	Number of poles	30
Number of phases	3	Slots/pole/phase	2/5
Series turns	108	Number of turns/coil	18
Number of coils	6	Number of parallel paths	1
Outer diameter	280 [mm]	Active length	60 [mm]
Total length	72 [mm]	Slot fill factor	35%
Slot opening width	2 [mm]	Slot bottom width	10[mm]
Slot top width	14.6[mm]	Slot opening height	3 [mm]
Slot height	25.4 [mm]	Back iron depth	9 [mm]
Tooth width	11.4 [mm]	Phase resistance	63[mΩ]

TABLE II: Rotor Dimensions for the 36-slot/30-pole SPM Machine

Rotor outer radius	88.6 [mm]	Magnets outer radius	101.6 [mm]
Inner radius	63.6 [mm]	Air gap thickness	1 [mm]
Magnet depth	13 [mm]	Magnet span	11.4° [mech]

TABLE III: Calculated Inductances for the 36-slot/30-pole SPM Machine

Self inductance (including harmonic leakage)	225[μH]	Mutual inductance (including harmonic leakage)	~0
Self slot leakage inductance	805[μH]	Mutual slot leakage inductance	~0
Total self inductance	1.03[mH]	Net mutual inductance	~0

TABLE IV: Calculated Current and Magnet Parameters for the 36-slot/30-pole SPM Machine

Magnet Remanent Flux Density, B_r	0.55 [Tesla] @ 100ºC	Magnet relative permeability, μ_r	1.22
RMS PM flux linkage Ψ_m	34.8 [mWb-rms]	RMS Characteristic Current, $I_{ch} = \Psi_m/L_d$	33.8 [Arms]
RMS Rated Current, I_R	43 [Arms]	Flux-Weakening Index $FWI = I_{ch}/I_R$	0.79
Copper Current density	7 [Arms/mm²]	Air Gap Shear stress	3.1 [psi] =21 [kPa]

TABLE V: Breakdown of Material Mass for the 36-slot/30-pole SPM Machine

Copper mass	2.8 [kg]	Iron mass	12.6 [kg]
Magnet mass	3.6 [kg]	Total mass	19 [kg]

the machine lamination design to restore the *FWI* value to unity with the same rated current (43 Arms). A parametric study showed that, starting with the existing lamination, increasing the slot opening by 2mm (from 2 to 4mm) and reducing the slot opening height by 1 mm (from 3 to 2mm) changes the design characteristics sufficiently to meet the optimal flux-weakening condition. No other major modifications would be required to achieve this goal. However, a stator using this new lamination design has not been fabricated.
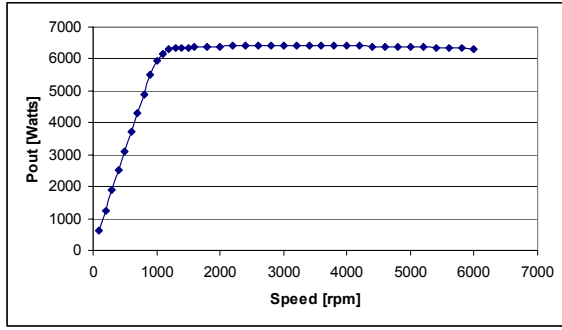
Figure 2: Calculated power vs. speed envelope of the prototype SPM machine
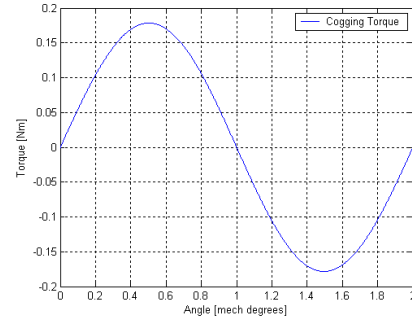

Figure 3: One cycle of the predicted SPM machine cogging torque
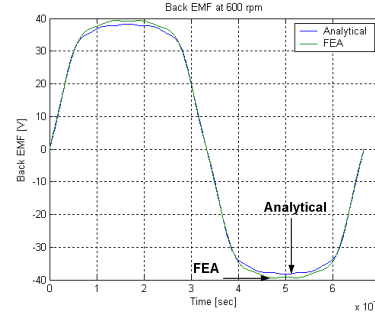

Figure 4: Overlaid analytical and FEA predicted phase back-emf voltage waveforms at 600 r/min
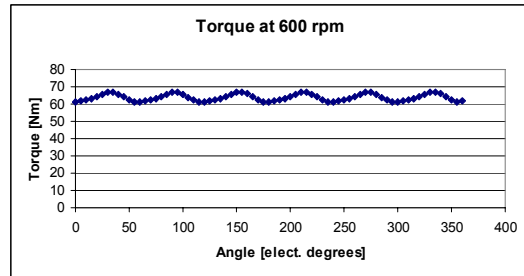

Figure 5: FEA predicted machine output torque at 600 r/min under sinusoidal current excitation.
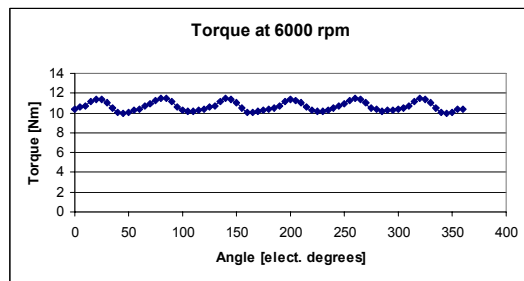

Figure 6: FEA predicted machine output torque at 6000 r/min under six-step voltage excitation

Updated analytical predictions for the prototype machine with the measured inductance (see Sec. VI) indicate that the required constant power level of 6 kW can still be achieved by increasing the dc bus voltage from 126 V to 195 V as shown in the calculated power vs. speed envelope curve in Fig. 2. This will be confirmed by experimental results later in this paper. The important observation is that this prototype machine continues to offer the opportunity to confirm that a wide constant-power speed range can be achieved despite its non-optimal characteristic current value.

C. Cogging Torque

Figure 3 shows one cycle of the predicted cogging torque for the prototype 36s/30p SPM machine. The predicted peak-to-peak cogging torque amplitude is less than 1% of the rated torque. This result is consistent with results presented elsewhere in the literature [1,11-13] showing that cogging torque is one of the significant advantages of using fractional-slot concentrated windings.

D. Finite Element Analysis Results

Figure 4 shows overlaid versions of the phase back-emf waveform at 600 r/min using both closed-form analysis and FEA. The excellent match between these two waveforms builds confidence in the accuracy of the analytical model. Although the phase back-emf waveform contains significant harmonic components, the triplen harmonics dominate so that little ripple torque is generated with three-phase sinusoidal current excitation. The line-to-line back-emf waveform is almost purely sinusoidal.

The ability of the prototype machine to achieve the desired high CPSR value has also been verified using FEA. Figure 5 shows the predicted output torque at 600 r/min over one pole pair using sinusoidal current excitation. The peak-to-peak ripple torque is less than 9% and the average developed output power is more than 4 kW. The predicted output torque at 6000 r/min under six-step voltage excitation is shown in Fig. 6, resulting in output power exceeding 6 kW.

The machine inductance calculated using FEA is 1.16 mH, in comparison to a predicted value of 1.03 mH using the improved analytical model. The error is approx. 11% which is quite acceptable taking into consideration the difficulty of accurately estimating the slot leakage in a machine with such a large effective air gap length.

III. ROTOR MAGNET LOSSES

Since the fractional-slot concentrated winding produces an airgap magnetic flux distribution that is rich in spatial subharmonics and higher-order harmonics [1], one of the key performance issues in such machines is the resulting eddy-current losses induced in the magnets and rotor core [14].
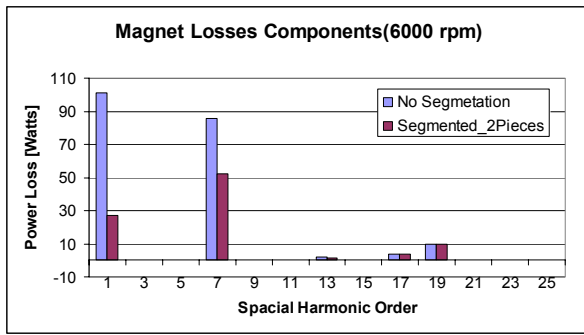
Figure 7: Predicted harmonic breakdown of magnet losses at 6000 r/min and the effect of segmentation.

In this prototype machine, the rotor core is laminated in order to minimize the eddy-current losses. The magnets selected for this machine are bonded NdFeB magnets that have a resistivity higher than 20 μΩm. Since bonded magnets have significantly higher resistivity than sintered magnets (0.5-1.5 μΩm), the choice of bonded magnets is important for minimizing the magnet losses in this machine.

The tradeoffs associated with selecting the lower-strength bonded magnet material include an increase in magnet mass (due to the increase in magnet depth), and a slight increase in the machine rated current for the same rated torque. Both of these factors contribute to a slight decrease in the machine's specific torque density [Nm/kg] compared to a comparable SPM machine designed using high-strength sintered magnets.

The magnet losses have been evaluated using both closed-form analysis [14] and FEA. A good match has been achieved between the predicted losses using both techniques. The predicted average magnet losses at 6000 r/min is approximately 230 W which is less than 4% of the machine output at this speed. This result is an important factor in the machine's ability to achieve high machine efficiency (over 90%) at high speeds. The 6000 r/min operating point represent the highest magnet losses since these losses are proportional to the square of the speed [14].

An option for further reducing the eddy current losses is segmentation of the magnets along the rotor periphery. This option has been investigated both analytically and using FEA, and the results are summarized in Fig. 7. This figure confirms the expectation that the dominant spatial subharmonics (in this case the fundamental and the 7th) are the primary sources of the magnet losses. This figure also shows that segmentation has a significant effect on reducing the loss components generated by these dominant subharmonics.

IV. INVERTER PERFORMANCE

The high pole number of this prototype (30) raises some concerns regarding the inverter performance, particularly at high speeds. Performance characteristics of the inverter power stage while exciting the prototype SPM machine have been calculated, including an investigation of the impact of the machine's high pole number on converter losses [15,16].

Since the minimum dc link voltage is approx. 200V, IGBTs were selected for the inverter switches. It is assumed that the
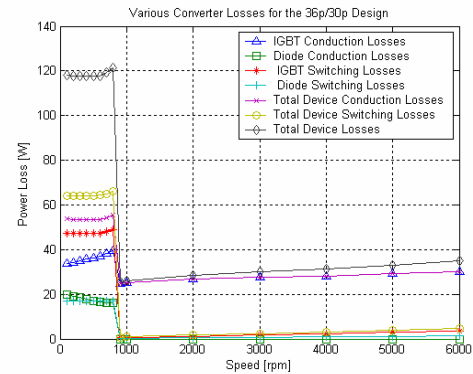

Figure 8: Predicted IGBT inverter loss components as a function of rotor speed along the machine capability envelope.
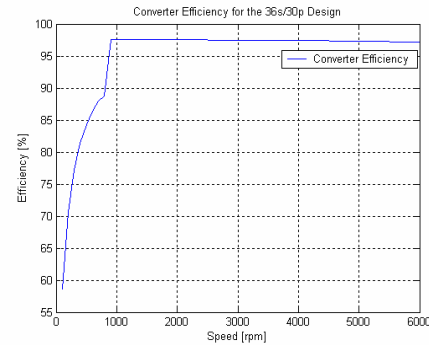

Figure 9: Predicted inverter efficiency along the machine capability envelope as a function of rotor speed

inverter operates in PWM mode with a switching frequency of 20 kHz at all rotor speeds below the adjusted base speed of 800 r/min, while six-step voltage excitation is applied at all higher speeds. As a result, the switching frequency equals the machine excitation frequency during high-speed operation.

The IGBT module used for this analytical exercise is manufactured by Fairchild Semiconductor [17] using 600V/75A IGBTs. Figure 8 shows the predicted inverter loss components as a function of speed along the machine's capability envelope, while Fig. 9 shows the corresponding inverter efficiency. It can be seen that switch conduction losses dominate at high speeds, and the inverter efficiency exceeds 95% throughout the constant-power operating regime. Below the base speed, the switching losses are more prominent since the converter is still operating in its PWM mode.

Another performance issue determined by the converter-machine interface is the amplitude of the phase current ripple. The maximum peak-to-peak current ripple amplitude can be estimated as follows [18]:

$$I_{ripple} = \frac{V_{dc}T_S}{4L_\sigma} \qquad (1)$$

where L_σ is the machine transient inductance, and T_S is the PWM switching period. This maximum ripple occurs when the machine phase is excited by a symmetrical square-wave voltage waveform (duty cycle = 0.5) with period T_S and amplitude $\frac{V_{dc}}{2}$.
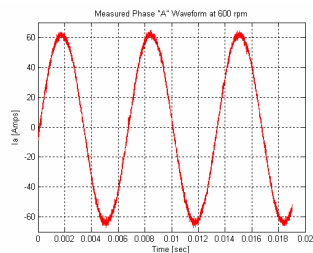
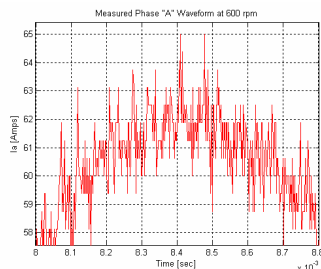Figure 10: Measured phase current at 600 r/min with rated current operation. V_{dc} = 300V

Figure 11: Expanded view of measured phase current at 600 r/min showing peak ripple.
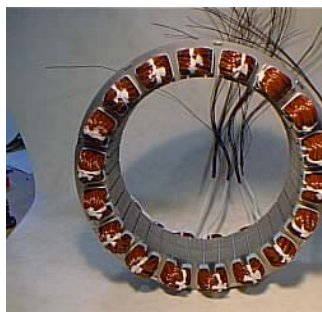

Figure 12: Prototype machine stator core and concentrated stator windings

Figure 13: Close-up view of concentrated winding with non-overlapping end turns

For SPM machine designs with concentrated windings, L_σ is equal to the machine phase self-inductance. For the prototype machine with a dc bus voltage of 300V and 20 kHz switching frequency, the predicted maximum current ripple is approx. 3A.

This value has been confirmed experimentally as shown in Figs. 10 and 11. Figure 10 shows the machine phase current at 600 r/min while Fig. 11 expands the interval where the maximum ripple occurs near the peak current. It can be seen that the current is quite sinusoidal and the peak-to-peak ripple is in the vicinity of 3A, as predicted. This ripple amplitude represents approx. 5% of the peak phase current which is quite acceptable. Additional calculations not presented here indicate that this low ripple contributes very little additional copper losses [19].

Figure 14: Rotor magnets during the assembly process

Figure 15: Rotor assembly showing hub, laminations, and mounted magnets

V. PROTOTYPE MACHINE FABRICATION & TEST CONFIGURATION

This section provides information about the prototype machine fabrication and test configuration. Figure 12 shows the laminated stator core and the concentrated winding coils. The stator lamination stack is held together using cleats. The thin back iron made possible by the high number of poles is also evident. Figure 13 highlights the concentrated stator windings and their short non-overlapping end turns.

Figure 14 shows the rotor assembly during fabrication including the aluminum inner hub, the rotor laminated core, and three of the assembled magnet poles. The rotor laminations are held together using axial bolts. The magnets are positioned on the rotor surface with the aid of small location guides on the periphery of the rotor laminations. The magnets are then fixed in place using glue and two layers of fiberglass tape. Each pole is divided axially into 3 magnet pieces due to magnet manufacturing limitations. Figure 15 shows the rotor after all the magnets were mounted.

Figures 16 and 17 show two different views of the prototype machine. In these figures, the stator has been installed inside the aluminum C-Core open frame. The rotor has also been mounted on the shaft and the bearings are visible in Fig. 18.

A schematic of the test configuration is shown in Fig. 18 [20]. The prototype 6 kW SPM machine is coupled to a flexible 4-quadrant dynamometer that uses a 25kW, 6000 r/min induction machine. An in-line torque transducer is used to measure the torque and speed. Each machine is excited by a 50 hp Danfoss drive controlled using a dSpace 1103 board.

Figure 16: Close-up view of the machine after stator-rotor assembly in frame

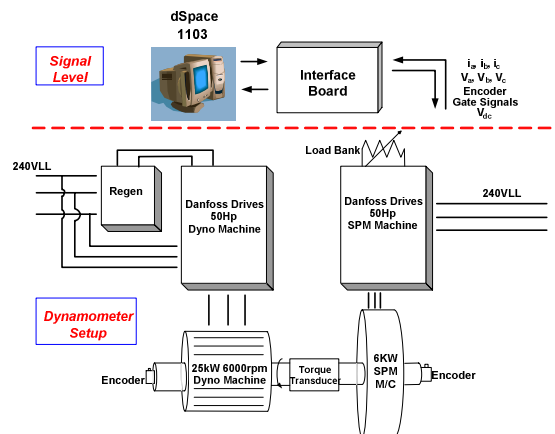Figure 17: End view of the machine after assembly, including bearings.

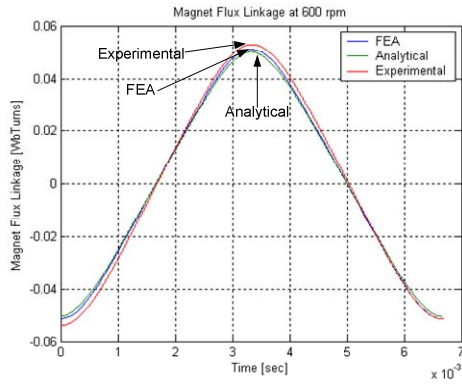Figure 18: Dynamometer test configuration for prototype SPM machine [20]

Figure 19: Comparison of calculated and measured phase *A* magnet flux linkage waveforms
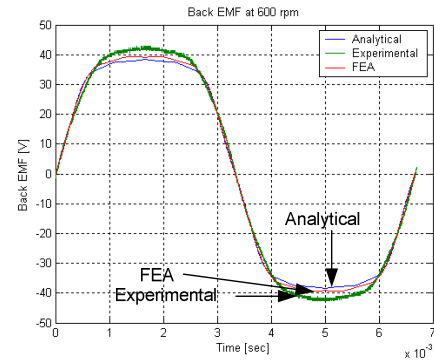

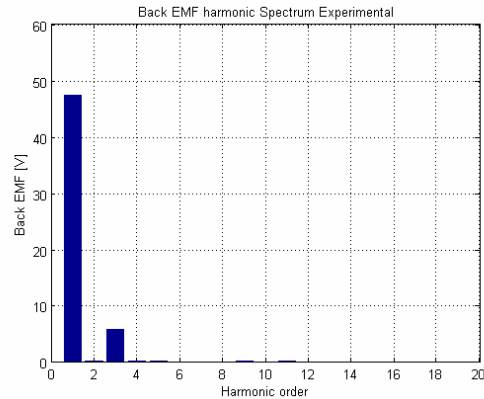Figure 20: Comparison of calculated and measured phase *A* back-emf voltage waveforms at 600 r/min

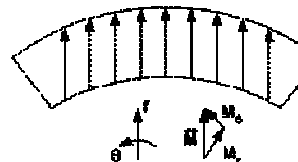Figure 21: Harmonic spectrum of the measured phase *A* back-emf voltage waveform at 600 r/min

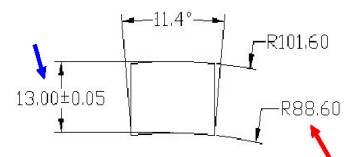Figure 22: Shape of the magnets used in the analytical model

Figure 23: Actual shape of the magnets used in the prototype machine

VI. EXPERIMENTAL RESULTS

This section provides a summary of the key experimental results, including parameter measurements and comparisons between the experimental results and both the closed-form analytical and FEA results.

A. Machine Parameters

The measured value of the stator phase resistance at room temperature is approx. 71 mΩ, 11% higher than the analytical prediction of 63 mΩ . The main reason for this discrepancy is the difference between the 40% copper slot fill factor used in the calculations and the actual achieved value of approx. 35%.

The measured phase inductance is approx. 1.3 mH which is higher than both the updated analytical prediction (1.03 mH) and the FEA prediction (1.16 mH). Sources of this difference include the end leakage inductance that is not included in either the 2D FEA or the analytical predictions, and remaining inaccuracies in the slot leakage inductance estimate.

Figure 19 shows the measured phase *A* magnet flux linkage compared to both the analytical and FEA results, demonstrating very good matches in both cases. The experimental flux linkage is slightly higher than either of the analytical results due to the fact that the actual magnet B_r value of the received magnets is approx. 0.59T at room temperature compared to the magnet B_r design value of 0.55T at 100°C.

Figure 20 shows the measured phase *A* back-emf voltage compared to both the closed-form analytical and FEA results, again demonstrating very good matches. As in the case of the flux linkages, the slightly elevated amplitude of the experimental back-emf is attributable to the difference in B_r.

The measured harmonic spectra of the experimental back-emf waveform is shown in Fig. 21. It can be seen that the measured back-emf waveform consist almost entirely of a fundamental and a 3rd harmonic component. The analytical back-emf waveform includes some higher-order harmonic components in addition to the fundamental and 3rd harmonic components. This favorable result suggests that the prototype machine will have lower torque ripple than predicted. With a floating neutral winding connection, the 3rd harmonic component in the back-emf voltage is prevented from

contributing any ripple torque since triplen harmonic currents cannot flow.

The small difference between the measured and predicted back-emf harmonic spectra can be explained by comparing the magnets shape used in the analytical model shown in Fig. 22 [21] and the actual magnet shape used in the prototype machine shown in Fig. 23. While parallel magnetization is used in both cases, the edges of the actual magnet are slightly tapered compared to the assumed analytical shape due to manufacturing constraints. This tapered magnet shape is responsible for the near-absence of higher-order harmonics in the measured back-emf voltage waveform.

B. Machine Torque and Power vs. Speed Envelopes

As discussed previously in Section II, the dc bus voltage was raised from its original design value of 126V to 195V as a
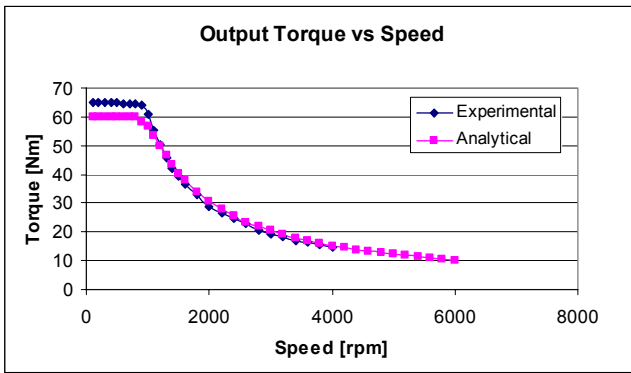
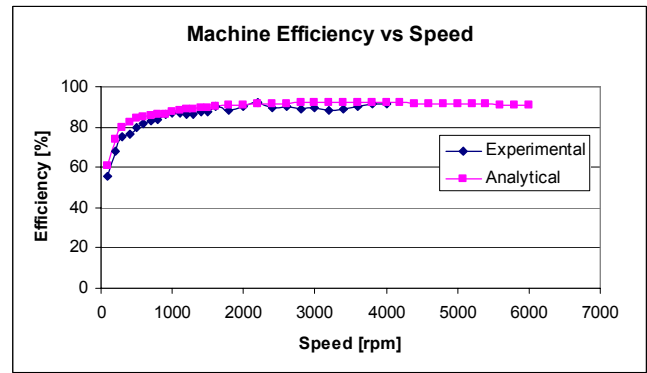Figure 24: Comparison of the measured and calculated machine torque vs. speed envelopes

Figure 25: Comparison of the measured and predicted machine power-speed envelopes

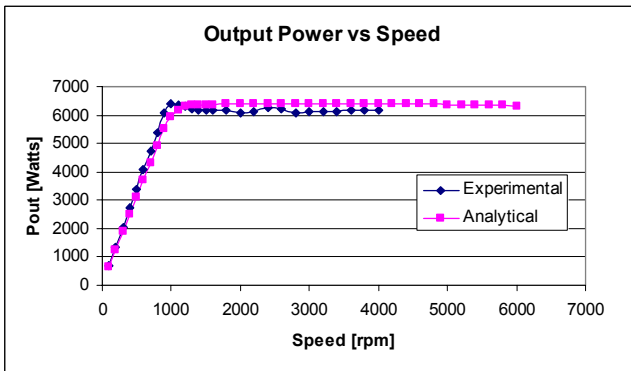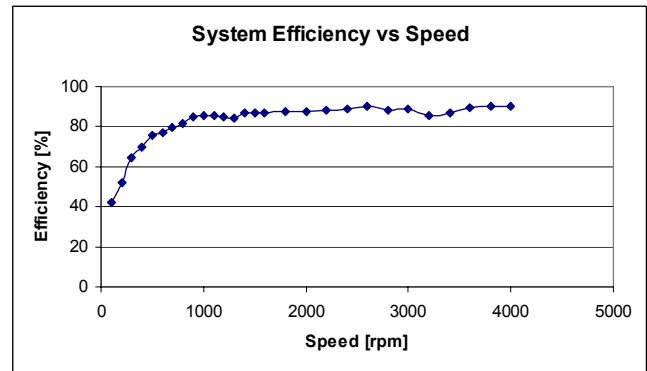Figure 26: Comparison of the measured and calculated machine efficiency vs. speed envelopes

Figure 27: Measured machine-plus-inverter system efficiency vs. speed envelope

Figure 28: Comparison of the measured and calculated inverter efficiency vs. speed envelopes

result of the higher-than-expected phase inductance. This higher bus voltage makes it possible to demonstrate that the machine can achieve a wide speed range of constant-power operation at the 6 kW level.

For the test results reported here, the bus voltage was raised to a somewhat higher value than the minimum required value of 195V, and the tests were conducted with the machine operating continuously in PWM mode in order to simplify the control issues. The torque/power envelope tests were carried out by adjusting the synchronous-frame i_d and i_q current values to develop the desired torque/power within the targeted phase voltage limit of 87.8 Vrms (fundamental). This phase voltage corresponds to a dc link bus voltage of 195V (ignoring switch voltage drops) with six-step voltage excitation (i.e., $195*\sqrt{2}/\pi = 87.8$ Vrms).

Comparisons of the measured and updated analytical machine torque vs. speed envelopes and the corresponding power vs. speed envelopes are shown in Figs. 24 and 25, respectively. . The envelope curves in Figs. 24 and 25 show that there is a very good match between the measured and analytical results up to the maximum test speed of 4000 r/min. These results are very significant since they confirm that the prototype machine has achieved a wide speed range of constant-power operation (approx. 5:1, to date).

At the time of this writing, no tests have been carried out above 4000 r/min in order to complete testing at lower speeds before exposing the rotor to higher structural stresses. All
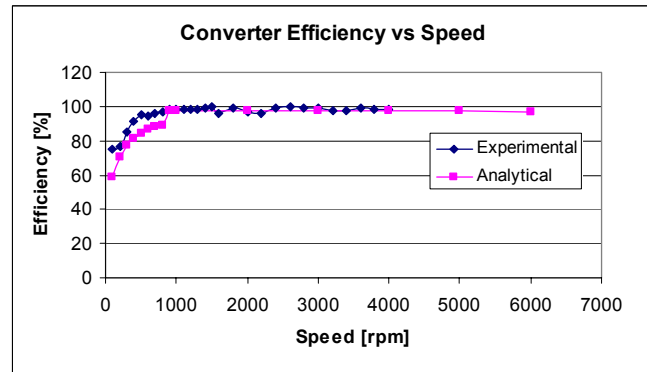
available evidence suggests that the machine will be able to demonstrate higher CPSR values before testing is completed.

The results in Fig. 24 show that the measured torque is slightly higher than predicted at lower speeds for the same stator current. This is consistent with the higher value of magnet B_r in the prototype machine, as previously discussed.

C. Machine and Inverter Efficiency vs. Speed Envelopes

Figure 26 shows a comparison of the measured and calculated machine efficiency vs. speed along the maximum torque/power envelope. Updated analytical predictions and measured results agree very closely over the entire tested

speed range up to 4000 r/min. The measured prototype machine efficiency is higher than 90% at elevated speeds, confirming successful suppression of the eddy current losses in the magnets and rotor core that are generated by the significant airgap subharmonic field components. This is very significant since these losses have been considered to be one of the key potential obstacles to using fractional-slot concentrated windings for high-speed operation.

Figure 27 shows the measured machine-plus-inverter system efficiency vs. speed envelope. The inverter input power was determined using measurements of the dc bus voltage and current. The output power was determined by measuring the machine output torque and speed. This curve shows that the machine-plus-inverter efficiency is nearly 90% over most of the speed range up to 4000 r/min, confirming the opportunities provided by the concentrated winding SPM machine to achieve high drive efficiency values.

Using the measured machine and system efficiency values presented in the preceding two figures, the "measured" converter efficiency has been extracted and compared to the analytical predictions in Fig. 28. Consistent with the results in Figs. 26 and 27, the predicted and measured inverter efficiency values agree very well, reaching values in the vicinity of 98% at high speeds.

VII. CONCLUSIONS

A 6 kW 36-slot/30-pole fractional-slot concentrated winding SPM machine has been successfully designed, fabricated, and tested to achieve a wide speed range of constant-power operation. Closed-form analysis and FEA have been used extensively during the design process. Important machine and drive performance issues including the eddy current losses in the magnets and the inverter losses have been analyzed in detail.

Experimental results from the prototype SPM machine were used to improve the accuracy of the closed-form analytical model for machine inductance calculations. Comparisons between the machine parameters and performance derived from the improved analytical model, FEA, and the experimental tests have demonstrated very good agreement.

The test results have convincingly demonstrated the SPM machine's ability to deliver wide speed ranges of constant-power operation as well as high machine efficiency. These experimental verification results are intended to assist PM machine and drive designers who are interested in considering SPM machines for applications such as electric traction that have generally been considered beyond its reach in the past.

ACKNOWLEDGEMENT

REFERENCES

[1] A.M. EL-Refaie, and T.M. Jahns, "Optimal Flux Weakening in Surface PM Machines Using Concentrated Windings", *IEEE Trans. Ind. Appl.*, vol. 41, May-Jun 2005, pp. 790-800.

[2] A.M. EL-Refaie, and T.M. Jahns, "Analysis of Surface Permanent Magnet Machines Equipped with Concentrated Windings", accepted for publication in the *IEEE Trans. Energy Conversion*.

[3] J. Cros, J.R. Figueroa, P. Viarouge, "BLDC Motors with Surface Mounted PM Rotor for Wide Constant Power Operation", in *Rec. of 2003 IEEE Industry Applications Society Annual Meeting*, vol. 3, Salt Lake City, UT, October 2003, pp. 1933-1940.

[4] F. Magnussen, P. Thelin, and C. Sadarangani, "Performance evaluation of Permanent Magnet Synchronous Machines with Concentrated and Distributed Windings Including The Effect of Field Weakening", in *Proc. of 2nd IEE International Conference on Power Electronics, Machines and Drives (PEMD 2004)*, vol. 2, March-April 2004, pp. 679-685.

[5] E.C. Lovelace, T.M. Jahns, J.L. Kirtley Jr., and J.H. Lang, "An Interior PM Starter/Alternator for Automotive Applications," in *Proc. of 1998 Intl Conf. On Elec. Machines (ICEM)*, Istanbul, 1998, vol. 3, pp. 1802-1808.

[6] D.W. Novotny and T.A. Lipo, *Vector Control And Dynamics of AC Drives*, Calderon Press Oxford, 1998.

[7] T. A. Lipo, *Introduction to AC Machine Design*, Wisconsin Power Electronics Research Center, University of Wisconsin, 1996.

[8] Z.Q. Zhu, D. Howe, and T.S. Birch, "Calculation of Winding Inductances of Brushless Motors with Surface-Mounted Permanent Magnets", *in Proc. Intl Conference of Electrical Machines (ICEM)*, Paris, 1994, pp. 327-332.

[9] Z.Q. Zhu, and D. Howe, "Winding Inductances of Brushless Machines with Surface-Mounted Magnets", in *Proc. Intl Electric Machines and Drives Conference (IEMDC)*, May 1997, pp. WB2/2.1 - WB2/2.3.

[10] Z.Q. Zhu, D. Howe, and J.K. Mitchell, "Magnetic Field Analysis and Inductances of Brushless DC Machines with Surface-Mounted Magnets and Non-Overlapping Stator Windings", *IEEE Trans. Magnetics*, vol. 31, no. 3, May 1995, pp. 2115-2118.

[11] J. Cros, P. Viarouge, "Synthesis of High Performance PM Motors With Concentrated Windings", *IEEE Trans. Energy Conversion*, vol. 17, June 2002, pp. 248-253.

[12] F. Magnussen, C. Sadarangani, "Winding Factors and Joule Losses of Permanent Magnet Machines with Concentrated Windings", in *Proc. of 2003 Intl Elec. Machines and Drives Conf. (IEMDC'03)*, vol.1, Madison, WI, pp. 333-339, June 2003.

[13] Z.Q. Zhu, D. Howe, "Influence of Design Parameters on Cogging Torque in Permanent Magnet Machines", *IEEE Trans. Energy Conversion*, vol. 15, no. 4, December 2000, pp. 407-412.

[14] K. Atallah, D. Howe, P.H. Mellor, and D.A. Stone, "Rotor Loss in Permanent-Magnet Brushless AC Machines", *IEEE Trans. Ind. Appl.*, vol. 36, Nov-Dec 2000, pp. 1612-1618.

[15] F. Casanellas, "Losses in PWM inverters using IGBTs," *IEE Proceedings-Electric Power Appl.*, vol. 141, pp. 235 - 239, Sept 1994.

[16] M. H. Bierhoff and F. W. Fuchs, "Semiconductor Losses in Voltage Source and Current Source IGBT Converters Based on Analytical Derivation," in *Proc. of IEEE 35th Power Electronics Specialists Conf. (PESC)*, vol. 4, Aachen, Germany, pp. 2836 - 2842, June 2004.

[17] "FMG1G75US60H – Molding Type IGBT Module," Fairchild Semiconductor Data Sheet, 2002.

[18] J.W. Kolar, T.W. Wolbank, and M. Schrodl, "Analytical calculation of the RMS current stress on the DC link capacitor of voltage DC link PWM converter systems," in *Proc. of 9th International Conference on Electrical Machines and Drives (EMD99)*, pp. 81-89, 1999.

[19] A.H. Hava, "Carrier Based PWM-VSI Drives in the Overmodulation Region," PhD Thesis, Dept. of Electrical and Computer Engineering, University of Wisconsin-Madison, 1998.

[20] J. Wai, "High Performance Testbed for an Automotive Direct-Drive Starter/Alternator Synchronous Machine", MS Thesis, Dept. of Elec. & Comp. Eng., University of Wisconsin - Madison, 2002.

[21] Z.Q. Zhu, D. Howe, C.C. Chan, "Improved Analytical Model for Predicting the Magnetic Field Distribution in Brushless Permanent-Magnet Machines*", IEEE Trans. Magnetics*, vol. 38, Jan 2002, pp. 229-238.